Heritage Science

RESEARCH

Open Access

Cleaning testing of nineteenth-century plaster surface models with thin polyacrylamide-based gel layers attached to flexible polyethylene films

Charis Theodorakopoulos[1*], Valentina Risdonne[2], Silvia Freese[3], Samar Diraoui[3] and Ulrich Jonas[3]

Abstract

This paper explores the cleaning efficacy of polyethylene-supported 15-min photo-crosslinked poly (acrylamide-co-benzophenone) surface-attached gels (SAGs) on gypsum plaster surface models inspired by nineteenth-century casts. Cleaning tests were performed on plaster surface models with and without organic and inorganic coatings, which had been exposed to accelerated ageing by heat, humidity, and light after artificial soiling. The specific types of SAG systems were selected based on their water loading and dehydration capacities. The SAGs were loaded with customized solutions and applied on the plaster models for one minute. Cleaning efficacy was evaluated with visible reflectance, UV fluorescence photography, scanning electron microscopy, colorimetry, UV/Vis spectrophotometry, glossimetry, high resolution 3D microscopy, attenuated total reflection Fourier transform infrared spectroscopy and 2D Fourier transform infrared imaging. The SAGs provided fast and minimal wetting of the substrates, prevented excessive liquid spreading and allowed the effective liquid contact with the soiled gypsum plaster surface. A striking removal of soils from the gypsum plaster surface models was observed, which suggests convenient application of the SAG systems for the cleaning of historical plaster objects.

Keywords Surface-attached gels, Plaster surface models, Cleaning efficacy, Scanning electron microscopy, Colorimetry, Glossimetry, High resolution 3D microscopy, Attenuated total reflection Fourier transform infrared spectroscopy, 2D Fourier transform infrared imaging

Introduction

Gel technology is recognized as a relatively non-destructive cleaning technique in art and cultural heritage conservation [1]. Since water is the most common non-toxic cleaning solvent, hydrogels are developed for the controlled delivery of water and water-based solutions into the surface of heritage objects and artworks [2]. Optimal cleaning applications aim to not leave gel or reagent residues onto the artwork's surface, eliminate leaching of volatile constituents [3, 4] and reduce the required volume of the solution diffused into the substrate [5]. Natural polysaccharide hydrogels, such as agar gels [6], as well as synthetic systems, such as polyvinyl alcohol-based [7] and poly(2-hydroxyethyl methacrylate)/poly(vinylpyrrolidone) semi-interpenetrating polymer network hydrogels [8] have eliminated polymer residues, which was a side-effect of the gel-like materials and solutions that were utilised in the past [9]. Handling and retention properties were also improved, thus enhancing

*Correspondence:
Charis Theodorakopoulos
charis.theodorakopoulos@northumbria.ac.uk
[1] Department of Arts, Science in Conservation of Fine Art, Northumbria University, Newcastle Upon Tyne NE1 8ST, UK
[2] Collection Care and Access, Victoria and Albert Museum, London SW7 2RL, UK
[3] Department Chemistry - Biology, University of Siegen, Adolf-Reichwein-Strasse 2, 57076 Siegen, Germany

the cleaning of selected surfaces. Another tested hydrogel-forming material is polyacrylamide, which is characterised by a strong polymeric network with improved mechanical properties [10].

Upon uptake of water-based solutions these materials form bulk hydrogels that are expanded in three dimensions diffusing the aqueous medium through the interface with the substrate [11]. The bulk polymer network of hydrogels generates an open structure with a large inner surface that can take up some 100-fold amounts of water-based solutions [12]. The release of the solution content depends on the capillary action between the polymer network and the substrate, which is related to the porosities of both the polymer network and the surface, the surface roughness of the latter and its composition [13]. However, given that bulk gels can be thicker than the surfaces to be cleaned by at least 3 orders of magnitude (at least a few mm gel film over surface layers of a few microns), there is an excess of solution released, with the risk of diffusing more liquid than necessary for the cleaning procedure [14]. To reduce the liquid volume, we introduced customisable surface-attached gel (SAG) systems [15, 16], which are typically 2–5 μm thin poly(acrylamide)-based (PAM) hydrogel films that are covalently bonded to transparent and flexible polyethylene (PE) backing films via photo-crosslinking of benzophenone acrylamide (BPAAm) that is incorporated in the polymer network. The PE backings provide flexibility and stability, simplify handling and allow the user to clearly observe the cleaning progress through the SAG system while it is on a surface [15]. Moreover, the optional co-polymerisation of acrylate monomers of poly(oxyethylene) lauryl ether (Brij35), or 2-(2-((2-ethylhexyl)oxy)propoxy)ethan-1-ol (Ecosurf EH-3 and EH-9) surfactants in the network [16] controls the degree of hydrophilicity and lowers the surface tension of surfactant-free aqueous solutions while the gel system is in contact with the substrate [17].

The adjustable malleability of the PE-PAM-based gel layers (via the crosslinking step), and the roughness of the substrate are important for the effectiveness of the gel-surface contact [16]. Upon contact the liquid releases and the cleaning action is faster compared to bulk gels. This is because of the following inherent properties of surface-attached gels: 1. the quasi-one-dimensional intense swelling/collapsing of the polymer network due to the immobilisation of one side of the gel layer on the backing film, which further enhances the contact with the substrate, and 2. the minute amount of solution contained in the thin gel matrix that is released fast upon the intense swelling of the free side of the gel layer [11]. Documented cleaning trials have demonstrated that a 1-to-2-min contact of PE-PAM-based copolymer or terpolymer hydrogels effectively removed dirt from low molecular weight resin films, an aged mastic varnish from tempera paint, while one touch applications of the PE-PAM systems co-polymerised with Brij35 acrylate thinned the dammar varnish of a nineteenth century painting [15, 16]. In the latter case, the degree of depth-step thinning was related to the duration of photo-crosslinking of the polymer network and the concentration of the swelling solution of the gel layer of the SAGs.

The scope of this paper is to expand testing of SAG cleaning to yet unexplored models of gypsum plaster surfaces coated with drying oils, resins, barites and/or waxes; these coating materials were historically used for improving the surface properties of porous materials used in cultural heritage [18]. Due to the complex characteristics of the plaster surfaces, the removal of accumulated dirt from delicate historical plaster casts [19] or other similar cultural heritage surfaces requires consideration of several factors related to: 1. the physical features of plaster surface, such as absorptivity to water and aqueous solutions, porosity, fragility, embrittlement and water solubility [20], 2. the presence and types of coatings which were originally used as protective and appearance controlling layers, and 3. the presence of non-original adhesives, coatings or paints added in restoration/conservation procedures. Cleaning tests of nineteenth-plaster casts at the Victoria and Albert Museum (V&A) [21] included: soft brushing together with the use of vacuum cleaner or the use of PVC sponges, vulcanised rubber sponges, microfibre cloth, phthalate-free and latex-free erasers; swab-rolling with solutions of varying polarity and water; and the use of pulps based on cellulose derivatives, latex poultices, or agar gels. These methods showed a wide range of cleaning efficacies [21]. In search of an efficient cleaning treatment, the performance of a pilot cleaning procedure with PE-PAM SAG systems swollen on tailored water-based solutions was investigated. Herein we report the findings of this investigation.

Experimental

Materials

For the samples calcium sulphate dihydrate, $CaSO_4{\cdot}2H_2O$, gypsum powder (Formula Saint Gobain Fine Casting Plaster), cold-pressed linseed oil (C. Roberson & Co., Code: CR32225J), boiled linseed oil (Kremer Pigmente, 79424), white shellac resin (Kremer Pigmente, 60471), barium hydroxide octahydrate, $Ba(OH)_2 \cdot 8H_2O$ (Kremer Pigmente, 64080), calcium hydroxide, $Ca(OH)_2$ (Sigma-Aldrich CAS No.: 1305-62-0), bleached beeswax (Kremer Pigmente 62210, CAS No: 8012-89-3), purified oil of turpentine (Merck 24245, CAS No: 8006-64-2) were used as received.

The dry portion of the soiling mixture consisted of carbon black pigment (Kremer Pigmente, 0.23 wt%), iron

oxide pigment (Kremer Pigmente, 0.06 wt%), gelatine powder (VWR, code number: 24350, 1.14 wt%), soluble starch (1.14 wt%), Portland Type I cement (B&Q Blue Circle Mastercrete Handy Pack Cement, 1.99 wt%), silica gel (Sigma-Aldrich Fumed Silica gel powder, S5130, 0.20 wt%), kaolin (Kremer Pigmente, 58250, 2.28 wt%). The wet portion of the mixture consisted of high-grade mineral (paraffinic) oil (Sigma-Aldrich, 18512, 1.82 wt%), olive oil (1.05 wt%) and white spirit (SLS scientific laboratory supplies, CHE3886, 90.09 wt%).

For the solutions, glacial acetic acid, HOAc, (VWR Chemicals BDH), sodium hydroxide, NaOH, concentrated hydrochloric acid, HCl, (Honeywell Fluka), citric acid (CA), ethylenediaminetetraacetic acid (EDTA) (Sigma-Aldrich), Industrial Methylated Spirit, IMS 99% (v/v), Pure and triethanolamine (TEA) (99%) (Fisher scientific) were used as received. Gensieve LE agarose powder (cat no. H19365) was used as received. Deionised (DI) water (pH 6.9, 18.3 °C, 0.007 mS/cm) was used in all tests.

Poly(acrylamide-co-benzophenyl acrylamide) and poly(acrylamide-co-Ecosurf-3 acrylate-co-benzophenyl acrylamide) films covalently attached to a transparent polyethylene film by photo-crosslinking for 15, 30 and 60 min (PE-PAM_{15}, PE-PAM_{30}, PE-PAM_{60} and PE-$PAME_{15}$) were stored from a previous study [16]. The films were immersed in water and dried for 3 days before use.

Sample preparation

The reconstructed gypsum plaster plates were based on the materials characterized on 12 V&A plaster casts produced in the nineteenth century by the Küsthardt, Notre-Dame and Franchi workshops [22]. Multianalytical studies [23] characterised the materials and revealed the simple stratigraphy of the selected casts, made of gypsum plaster and coatings [18, 22–25]. In line with historical treatises [18] organic coatings such as shellac resin, linseed oil, beeswax and inorganic coatings such as barites were identified in the original casts [23]. Based on these findings, gypsum plaster plates were made of 50 wt% calcium sulphate dihydrate, $CaSO_4{\cdot}2H_2O$, gypsum powder in DI water. These were then coated in two distinct areas with the same or similar material (Additional file 1: Fig. S1).

Prior to the application of coatings, the plates were dried for 50 days at room temperature (RT) in the laboratory. The dry plaster plates were coated with:

- 2 coats of cold-pressed linseed oil (CL),
- 2 coats of boiled linseed oil (BL),
- 2 coats of 6 wt% white shellac resin in IMS (SR6),
- 2 coats of 18 wt% white shellac resin in IMS (SR18),
- 6 coats of $Ba(OH)_2 \cdot 8H_2O$ (5.58 g, 17.69 mmol) blended with $Ca(OH)_2$ (0.24 g, 3.24 mmol) in 100 mL DI water stirred at RT (BC),
- 6 coats of 5 wt% $Ba(OH)_2 \cdot 8H_2O$ in DI water solution stirred at 60 °C (BA)

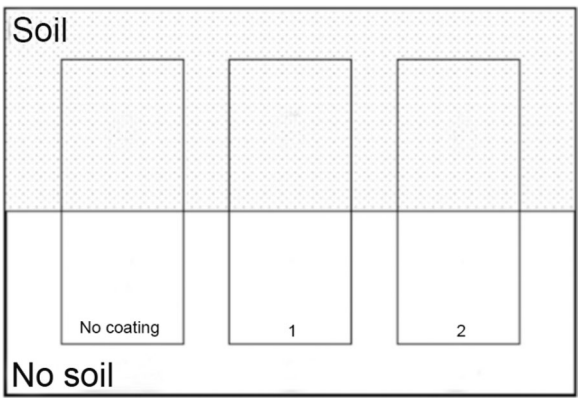

Scheme 1 Layout of gypsum plates with coatings and soils (upper part) and unsoiled coatings (lower part)

The coated plates were subjected to the following curing/ageing procedure [22]: dried for 129 days at RT, then exposed to 45% RH and 40 °C for 28 days. Then, some of the coated and uncoated (uc) plates were soiled. For the soiling process the solid materials listed above were finely crushed in a blender and dispersed in the mineral oil mixture, as reported in previous work [26]. The plaster model surfaces were sprayed with the soiling mixture, and after drying subjected to 45% RH, 40 °C for 35 days. The unsoiled samples were further coated with 2 coats of a 1:1 solution of bleached beeswax (WX) and oil of turpentine, which was applied at 60 °C. Then half of the waxed samples were soiled. Then, all soiled unsoiled and waxed coated plates received a 114.5 Mlux.hrs light dose in the xenon-arc fadeometer.

Each gypsum plate had two coated areas and was organized as shown in Scheme 1. The coatings were applied in areas 2 and 3. For example, a plate was coated with cold-pressed linseed oil (CL) in area 1 and boiled linseed oil (BL) in area 2. Similarly, the other plates were coated with SR6 in area 1 and SR18 in area 2 or BC in area 1 and BA in area 2. Beeswax (WX) was applied on a separate gypsum plate with just one coat. The upper parts of the plates were soiled leaving the lower parts without soils.

Accelerated ageing

Exposure to temperature and humidity

A Mercia Scientific MGF8401 Excell Humidity cabinet MER 180 SCN/RH was used. The cabinet allows a

controlled temperature in a range of 10 to 40 ± 2 °C, and humidity up to 75 ± 5% RH with the aid of a humidified air source which circulates a micro-mist in the cabinet.

Exposure to light

A Q-Sun Xenon Xe-1 Test cabinet was used. The system has a single 1800W (X-1800) xenon-arc lamp (270–800 nm) that generates 1.0 W/m^2 irradiance at 420 nm and is equipped with daylight and window-Q filters. The filters reproduce the spectral power distribution (SPD) of sunlight in the low-wavelength region of the UV spectrum (CIE No. 85:1989) and simulate daylight through window glass according to BS EN ISO 16474-1:2013 [27]. The temperature inside the Q-Sun chamber did not exceed 40 °C.

pH and conductivity measurements

pH and conductivity (σ) of the unaged and aged plaster surfaces were measured by the use of agarose swollen in deionised (DI) water, Horiba LAQUA twin compact pH meter (LAQUA twin -pH-22, accuracy ± 0.1 pH) and Horiba LAQUA twin compact conductivity meter (LAQUA twin-EC-22, accuracy ± 2%). Agarose gel plugs were prepared upon dispersing 2 wt% agarose LE in DI water. The dispersion was microwaved at high heat for 30 s, stirred and heated 4 more times for 10 s each time. After cooling, the dispersion was heated for another 20 s and then poured on a silicon mould to set to the shape of a 4 mm thick disc. An agarose gel plug was cut with a 2.5 mm specimen puncher and left on the surface of the coated plaster mock-ups (Additional file 1: Fig. S2) for 2 min. Then, the gel plug was lifted with the aid of tweezers and placed in the pH meter, and then in the conductivity meter to record the respective readings of the coated and uncoated plaster surfaces. Table 1 shows the pH and conductivity readings, the tested solutions and the effective solutions that were loaded into the SAGs for the cleaning trials.

Cleaning treatment

To select the appropriate cleaning solution, shown in Table 1, a cotton swab carrying the solution was rolled at a discrete spot on the surface and when a satisfactory result was obtained the effective solution was used for incubation of the surface-attached gels (SAGs). Then, the swollen SAG pad (5 × 5 mm PE-PAM$_{15}$ and PE-PAME$_{3\text{-}15}$ SAGs) was placed on the plaster plate surface facing with the hydrogel side to the plate, and gently pressed with a cotton swab to the substrate. After 1 min of contact the SAG was removed with the help of tweezers. The remaining soils released were then removed by gently rolling a dry cotton swab over the treated surface (Scheme 2). Since there was no difference in the cleaned surfaces treated with PE-PAM$_{15}$ and PE-PAME$_{3\text{-}15}$ SAGs, the cleaning trials continued with the PE-PAM$_{15}$ systems on larger surfaces of 2 × 2 cm (Additional file 1: Fig. S3).

Table 1 Tested solutions according to the pH and conductivity of the soiled surface

	Surface	pH	σ (mS/cm)	Solutions*	
				Tested	Effective
	Uncoated gypsum plaster (uc)	**5.95–6.34**	**0.04–0.22**	**a, b, c, d, h**	**d**
Coatings	Cold pressed linseed oil (CL)	9.19	0.06	g, h	h
	Boiled linseed oil (BL)	6.71	0.03	b	b
	Shellac6% (SR6)	5.25	0.04	d, e	d
	Shellac18% (SR6)	5.27	0.08	a, d, e	d
	Barite with $Ca(OH)_2$ (BC)	9.00	0.12	a, c, h	h
	Barite 60 °C (BA)	8.54	0.04	a, c, h	h
	Beeswax (WX)	6.73–9.15	0.03–0.07	i	i

* Solutions

a. 0.11 M TEA buffered to pH 8 with 1 M acetic acid

b. 0.11 M TEA buffered to pH 8.5 with 1 M acetic acid

c. 0.38 M TEA buffered to pH 9 with 1 M HCl

d. 0.69 M HCl buffered to pH 6 with TEA

e. 0.09 M HOAc buffered to pH 5.5 with 1 M NaOH

f. 0.09 M HOAc buffered to pH 5 with 1 M NaOH

g. 2 wt% CA in DI water buffered to pH 8 with TEA

h. 2 wt% EDTA in DI water buffered with 1 M NaOH to pH 9

i. 70% (v/v) IMS in DI water

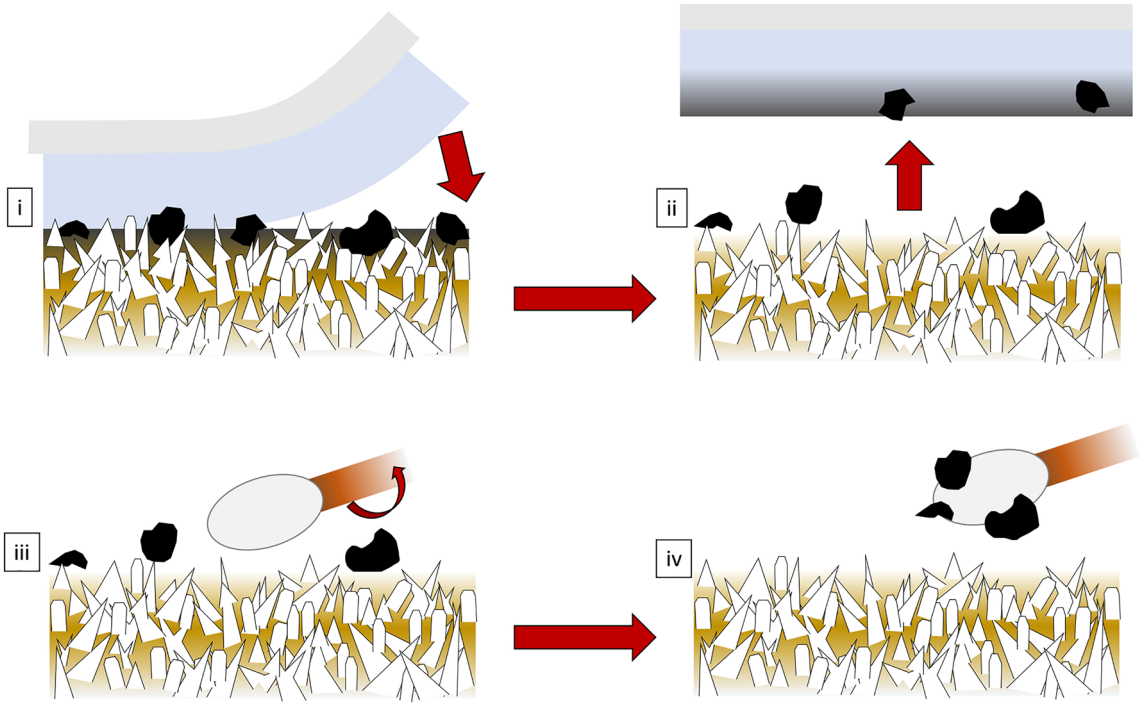

Scheme 2 SAG swollen in the effective aqueous solution was placed on the soiled plaster surface facing with the hydrogel side to the plaster (i). The SAG was removed after 1 min of contact leaving the plaster surface cleaner (ii). The remaining soil particles were then removed by gently rolling a dry cotton swab over the treated plaster surface (iii, iv)

Gravimetry

Gravimetric measurements were taken with a JJ-BC Series Electronic Analytical Balance (JJ224BC, capacity 220 g, resolution 0.1 mg). PE-PAM_{15}, PE-PAM_{30}, PE-PAM_{60} and PE-$PAM_{3\text{-}15}$ foils of 1.5 × 1.5 cm and average weight of 12 mg were swollen in DI water. After swelling, the foils were left for on minute until no further dripping of free water was observed. Then the surface-attached gels were brought in contact with a shellac resin film (6 wt% in IMS) and weighted every 5 s until no further weight reduction was detectable, which indicated the dehydration of the SAG systems.

Visible reflectance (VR) and ultraviolet fluorescence (UVf)

Visible light reflectance (VR) and ultraviolet fluorescence (UVf) images were recorded with a Canon EDS 6D camera. Two OSRAM DULUX L 55W/840 lamps and two NARVA LT36W/073 Blacklight Blue lamps were placed in 45/45° geometry for VR and UVf respectively. For the UVf images a Kodak Wratten 2E (52 mm Pitch: 0.75) was employed. Photos were calibrated using a Kodak Chart-13.

Scanning electron microscopy (SEM)

SEM was performed in a field emission TESCAN MIRA 3 SEM with a backscatter detector (BSE) in the Low Vacuum (10–15 Pa) Mode to obtain BSE images with the Bruker Alicona imaging software. Uncoated and coated plates with and without soils, and after cleaning were studied.

Colourimetry

A CM-2600d (Konica Minolta) spectrophotometer was used. The spectrophotometer operates with the specular component included (SCI) or excluded (SCE). At least three readings of the examined area were averaged. The instrument also obtained UV/Vis diffuse reflectance spectra within a wavelength range from 360 to 740 nm and the CIE$L^*a^*b^*$ colour space factors using the SpectraMagic NX software. The colour differences were calculated according to CIEΔE^*2000 [28] and the ASTM E313 Yellowness Index (YI_{313}) for D65/10° was determined [29]. The Whiteness Index (WI) (CIE 2004) [30] was not considered as the samples were not white enough to produce values within a valid range. Conversion equations to obtain YI_{313} and WI from the CIELAB measured coordinates, were run through the dedicated conversion codes for such provided by HutchColor (Copyright © 1995—endoftime HutchColor, LLC). The software provided the conversion but did not generate the experimental error. Nonetheless, the YI_{313} was considered as it provided a qualitative indication of yellowness.

Glossimetry

A Rhopoint IQ™ 20/60/85° Glossmeter/Goniometer was used. The readings of all samples resulted in less than 10 gloss units (GU) at 60° confirming visual observation of the matt appearance and therefore only the readings of the 85° sensor were considered. For the same reason the goniometry parameters that are only available with the 20° sensor for high gloss surfaces were not considered. Three measurements per surface were obtained and averaged.

High resolution (HR) 3D microscopy

A Bruker Alicona G5 Infinite Focus (IF) system was employed for HR 3D surface studies. The measurement on the plaster surfaces was taken with the 10×objective (vertical resolution 0.219 µm and lateral resolution 3.914 µm) and an area of 5.3×5.3 mm was measured. The system generates high resolution 2D and 3D images and generates roughness profiles and measurements of the average arithmetic roughness of the surface (Ra), the root mean square of the surface roughness (Rq) and the average of the tallest peak to the depth of the lowest valley from each or subsection of a surface measurement (Rz). The results were processed with the software Measure Suite 5.35.

Fourier transform infra-red spectroscopy (FTIR)

A Perkin Elmer Frontier FT-IR spectrometer (4000–350 cm^{-1} at the best resolution of 0.4 cm^{-1}) was used, equipped with a diamond crystal for ATR measurements and combined with a Spectrum Spotlight 400 FT-IR microscope equipped with a 16×1 pixel linear mercury cadmium telluride (MCT) array detector standard with InGaAs array option for optimised NIR imaging (7800–600 cm^{-1}). Spectral images from sample areas are possible at pixel resolutions of 6.25, 25 or 50 µm. A minimum of three spectra and IR spectral images were acquired in diffuse reflectance in the FTIR microscope (4000–650 cm^{-1}) followed by direct ATR surface analysis directly on the spectrometer (4000–350 cm^{-1}) using the Perkin Elmer Spectrum 10™ and SpectrumIMAGE™ software.

Digital optical survey micrographs

Prior to spectral image acquisition standard survey micrographs were obtained using the digital optical microscope incorporated in Spotlight 400 FT-IR system.

Results and discussion

A range of techniques was used to assess the changes on the soiled plaster surface after the application of the selected solution with the SAG systems, as described in the experimental section. BSE-SEM allowed to look at the morphology of the surfaces while digital optical survey micrographs highlighted the visual differences, and HR3D images allowed to determine the change in roughness. Reflectance and colorimetric measurement defined the degree of variation after cleaning. FTIR aimed to identify differences in chemical composition before and after cleaning, and to assess whether any residual soil and material from the SAG system was present.

BSE-SEM investigation of plaster surface models before cleaning

In order to investigate the effect of the cleaning process on the morphological features of the plaster surface, the plaster substrates before and after application of the SAG systems were observed by backscatter-scanning electron microscopy (BSE-SEM). The BSE-SEM micrographs (Fig. 1A) of the unsoiled and soiled plates demonstrate the tabular structure of gypsum plaster [31, 32]. No significant differences can be observed between the crystalline structures of the unaged and aged areas, aside from an increased presence of pores after ageing [23] generated upon drying during the accelerated ageing procedure. The BSE micrographs of the linseed oil (CL, BL) and shellac (SR6, SR18) coated plates show the tabular structure of gypsum plaster, although the mineral structure of the shellac coated plates appears tighter (Fig. 1A ii-v). The micrographs also show that the linseed oil (CL, BL) and shellac resin (SR6, SR18) coatings were absorbed and filled the pores of the gypsum plates and therefore these coatings did not form solid or uniform layers on top of the plates. Barite coatings (BC, BA) appear brighter due to the higher atomic mass of Ba compared to Ca. The structure on the barite coated plates appears tight and finer than the other samples in line with other observations [33]. Compared to the barite coating that was produced with calcium hydroxide at RT (BC), the neat barite coating (Fig. 1A vii) presented larger crystals grown upon the increased temperature (60 °C) that was required for its preparation. Finally, beeswax coatings (WX) covered the mineral structure of the plaster plates and formed a solid film on the plates. Soils on the aged uncoated and coated plaster plates appear as bright spots scattered across the surface and are in particular visible on the samples coated with linseed oil (CL, BL), shellac resin (SR6, SR18) and beeswax (WX) (Fig. 1B). These initial SEM observations formed the basis for the assessment of the cleaning efficacy which are discussed in more detail further below.

SAG dehydration tests

Dehydration tests based on the gravimetric measurements described in the experimental section were employed with the SAGs to estimate appropriate

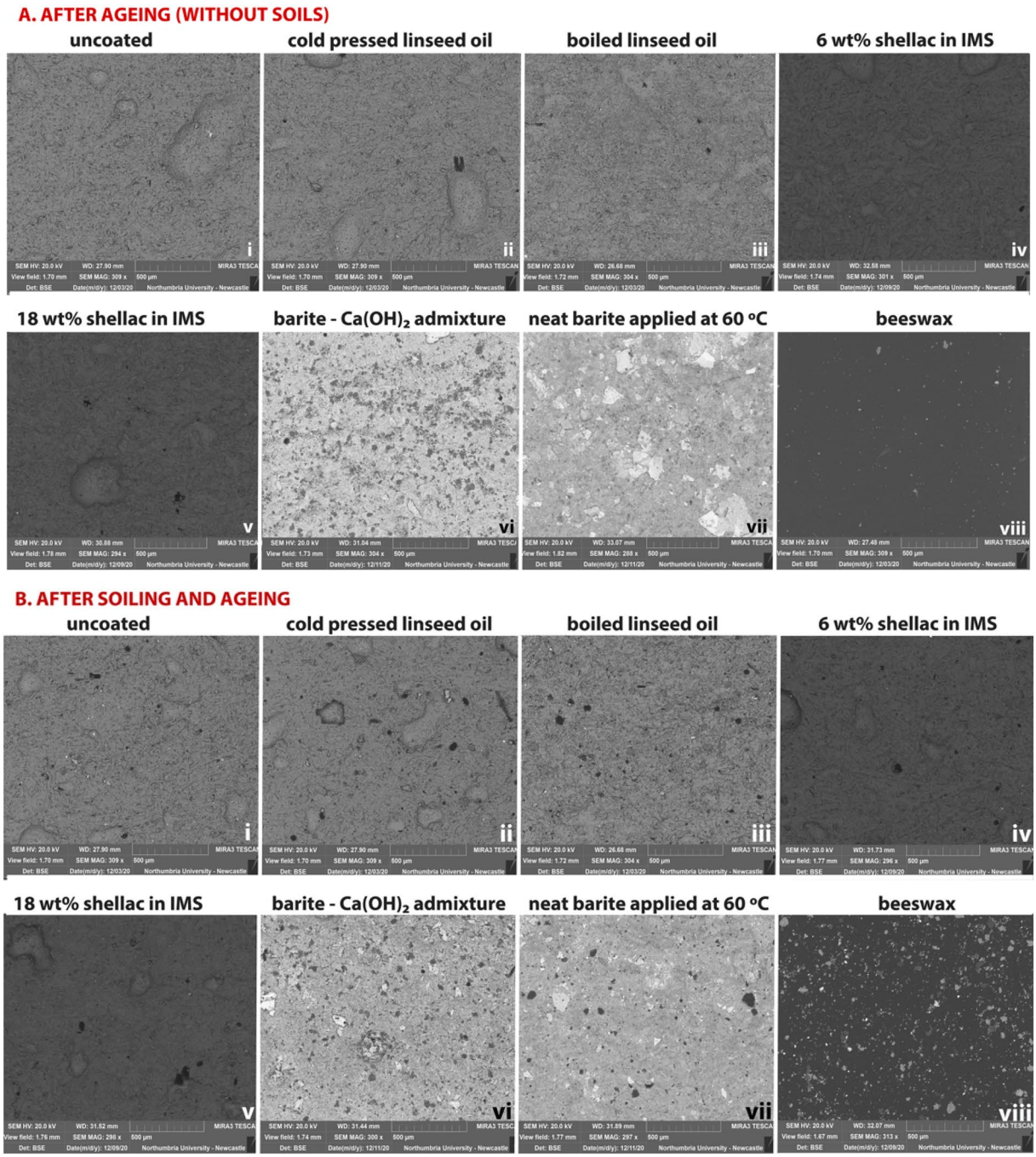

Fig. 1 BSE micrographs of the plaster surface models (**A**) after ageing without soils and (**B**) after soiling and ageing of (i) uncoated plaster (uc), and plaster coated with (ii) cold pressed linseed oil (CL), (iii) boiled linseed oil (BL), (iv) 6 wt% shellac in IMS (SR6), (v) 18 wt% shellac in IMS (SR18), (vi) barite with $Ca(HO_2)$ admixture (BC), (vii) neat barite (BA), and (viii) beeswax (WX)

contact times of the SAG on top of the plaster substrates. The PE-PAM_{15} and PE-$PAME_{3\text{-}15}$ SAGs released similar volumes of water than the more crosslinked films PE-PAM_{30} and PE-PAM_{60} SAGs, yet the latter two released water faster (Fig. 2), in line with previous observations [15]. Based on this study the cleaning trials were performed as described in the experimental section above.

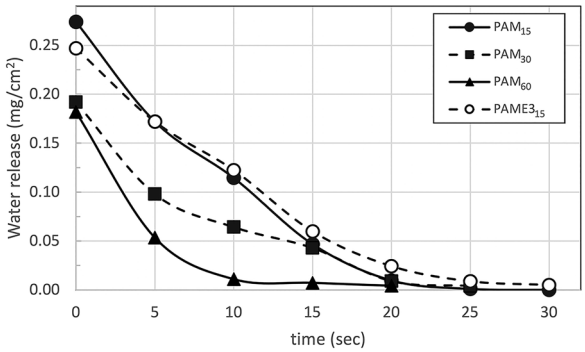

Fig. 2 Gravimetric dehydration of PE-attached PAM_{15}, PAM_{30}, PAM_{60} and $PAME_{3\text{-}15}$ SAG systems. Water release from PAM_{15} and $PAME_{3\text{-}15}$ was almost identical. PAM_{60} dehydrated faster than the other films tested

Post-cleaning surface evaluation studies

Comparison of the surfaces before and after cleaning was performed in order to assess the removal of the soil and whether any change occurred on the plaster model surface. The BSE micrographs after the cleaning trials are presented in Fig. 3, while Fig. 4 shows the test areas before and after cleaning in reflected visible light (VR) and UV fluorescence (UV*f*). All samples after cleaning appear brighter in visible reflectance and most samples show less features. In the UV*f* images the fluorescence increases after cleaning and more features are visible. This effect may be attributed to the quenching of fluorescence by the soil. The data demonstrate that the PE-PAM_{15} hydrogels achieved a remarkable removal of soil from the uncoated gypsum surfaces, as the appearance of the cleaned surfaces was closer to the unsoiled reference than to the appearance of the soiled surface. A relative unevenness of the removal of soil was expected due to the locally different absorption and porosity of the plaster surface which may have required more than one PE-PAM_{15} applications. The trials on the linseed oil (CL, BL) coated plates (Fig. 4B, C) were more effective than on shellac (SR6, SR18) coated plates (Fig. 4D, E) although these coatings were absorbed by the substrate. The plates coated with the barite solutions (BC, BA) responded to the cleaning procedure similarly to the uncoated plaster (uc) surfaces. A good cleaning efficacy was observed on the beeswax coated plates (Figs. 3, 4). Beeswax (WX) was the only material that formed a film on the substrate and therefore the contact with the PE-PAM_{15} removed soils effectively, similarly to previously reported tests on resin and varnish films [16]. The visible light and UV fluorescence observations indicated a successful soil removal in all cases.

Further evaluation of post-cleaning effects was achieved by comparing digital optical survey micrographs (Fig. 5) and HR 3D images (Fig. 6) of the surfaces to the BSE-SEM images (Fig. 3) discussed above. The reduction of soil particles from all plates is evident with

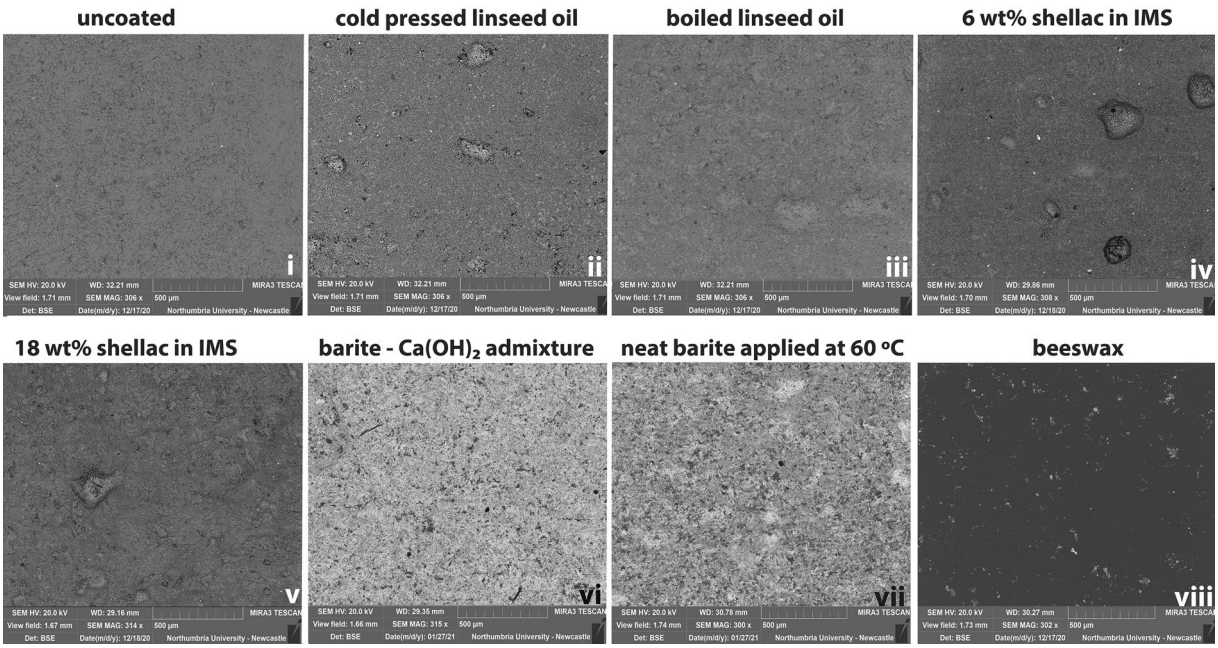

Fig. 3 BSE micrographs of the plaster surface models after the cleaning trials with PE-PAM_{15} SAGs of (i) uncoated plaster (uc), and plaster coated with (ii) cold pressed linseed oil (CL), (iii) boiled linseed oil (BL), (iv) 6 wt% shellac in IMS (SR6), (v) 18 wt% shellac in IMS (SR18), (vi) barite with $Ca(HO_2)$ admixture (BC), (vii) neat barite (BA), and (viii) beeswax (WX)

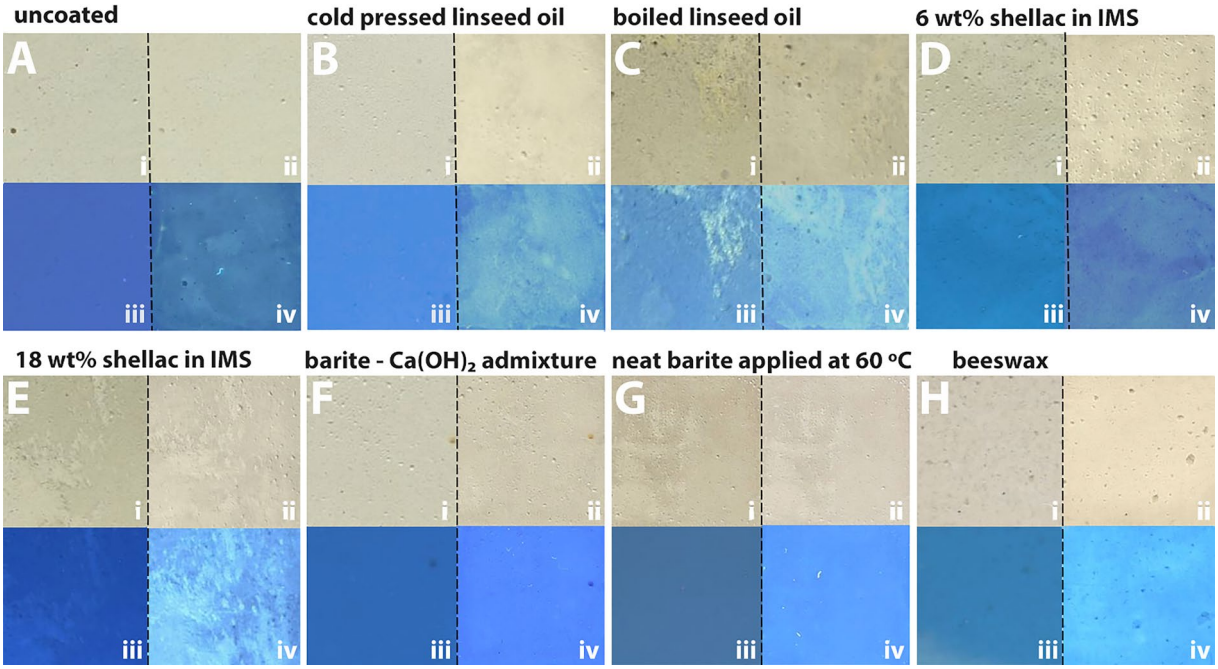

Fig. 4 Before (i, iii) and after (ii, iv) visible reflectance (i, ii) and UV fluorescence (iii, iv) images of the 2 × 2 cm surfaces of the aged unsoiled and soiled plates, **A** the uncoated plaster (uc) and (**B**–**H**) the plates with the following coatings: **B** cold pressed linseed oil (CL), **C** boiled linseed oil (BL), **D** 6 wt% shellac resin in IMS (SR6), **E** 18 wt% shellac resin in IMS (SR18), **F** barite with $Ca(OH)_2$ (BC), **G** neat barite (BA), and **H** beeswax (WX)

these methods. Upon cleaning, the uncoated (uc) plaster plates (cleaning performed with SAG swollen in aq. HCl-TEA solution—for composition refer to Table 1) and the plates coated with cold pressed linseed oil, CL, (SAG w/ aq. EDTA—NaOH solution, Table 1) and boiled linseed oil, BL, (SAG w/ aq. TEA- HOAc solution, Table 1) presented a slight surface smoothing which could be due to minor re-dissolution of the gypsum surface (Figs. 4, 5) despite the negligible volume of liquid released (Fig. 2). The plate coated with boiled linseed oil (BL) was not cleaned as effectively as the cold-pressed linseed oil, CL (Fig. 5). The surface of the shellac coated plates (SR6, SR18) cleaned with the HCl-TEA solution (Table 1) was less smoothed. The barite-coated plates (BC, BA) showed a reduced soiling removal when the EDTA-NaOH solution (Table 1) was used in the PE-PAM_{15} system (Fig. 5).

The HR 3D surface maps (Fig. 6) indicated the impact of the cleaning tests to the roughness of the plates (Additional file 1: Table S1). Detailed maps are included in a comprehensive database [23]. The cleaning efficacy of the PE-PAM_{15} systems is demonstrated by the post-cleaning reduction of roughness depth of all surfaces after the removal of soils. The average roughness, Ra, plots in Fig. 7 show that the uncoated plaster, and the plates coated with cold pressed linseed oil (CL) and barite with calcium hydroxide (BC) were smoother after the cleaning trials compared to the unsoiled plates. On the other hand, after the 1-min cleaning tests with the PE-PAM_{15} systems, the roughness of the plates coated with boiled linseed oil (BL), both shellac resins, SR6 and SR18, (based on the roughness depth, Rz) and neat barite (BA) were restored. The surface of the cleaned beeswax coated (WX) plate was the only sample that exhibited both higher average roughness, Ra, and roughness depth, Rz, compared to the unsoiled beeswax-coated (WX) plate. Nevertheless, the roughness of the beeswax surface under the soils might have been already increased by the containment of the soil particles prior to the cleaning trials. However, these differences are not significant considering the defects and the roughness of the uncoated plaster (uc) surface. Moreover, the deposition of soils followed by further accelerated ageing has altered the roughness of the underlying coated gypsum substrate compared to the surface prior to soiling [23]. In all cases, soiling increased the roughness. Yet, in the case of the 6 wt% shellac coating (SR6) the HR 3D data suggest a reduction of roughness depth after soiling (data shown in the supporting information, Additional file 1: Table S1). This is in contrast to the VR, the UVf (Fig. 4), and optical microscopy data (Fig. 5) for the SR6 plate. This discrepancy may be attributed to a saturation effect of the HR 3D camera by the SR6 coating with the intense illumination of the Alicona IF microscope. In the case of the beeswax coating (WX) the roughness depth was reduced after

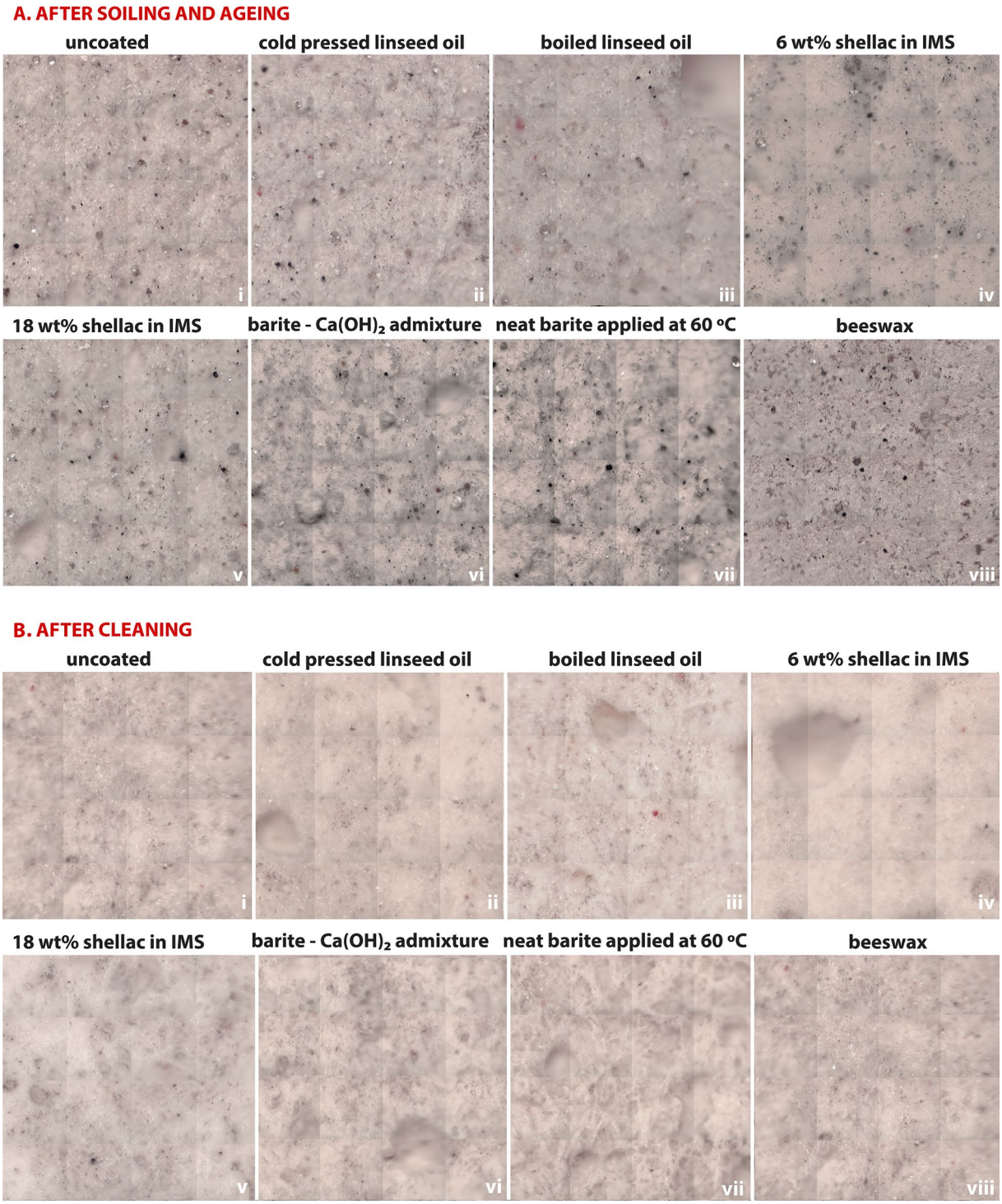

Fig. 5 Digital optical survey micrographs (1 × 1 mm) (**A**) after soiling and ageing (top row) and (**B**) after the cleaning trials with PE-PAM$_{15}$ SAGs (bottom row) of (i) uncoated plaster (uc) and plaster coated with (ii) cold pressed linseed oil (CL), (iii) boiled linseed oil (BL), (iv) 6 wt% shellac in IMS (SR6), (v) 18 wt% shellac in IMS (SR18), (vi) barite with Ca(OH$_2$) admixture (BC), (vii) neat barite (BA), and (viii) beeswax (WX). All micrographs are (**A**) after soiling and ageing, and (**B**) after the cleaning trials with the PE-PAM$_{15}$ SAGs

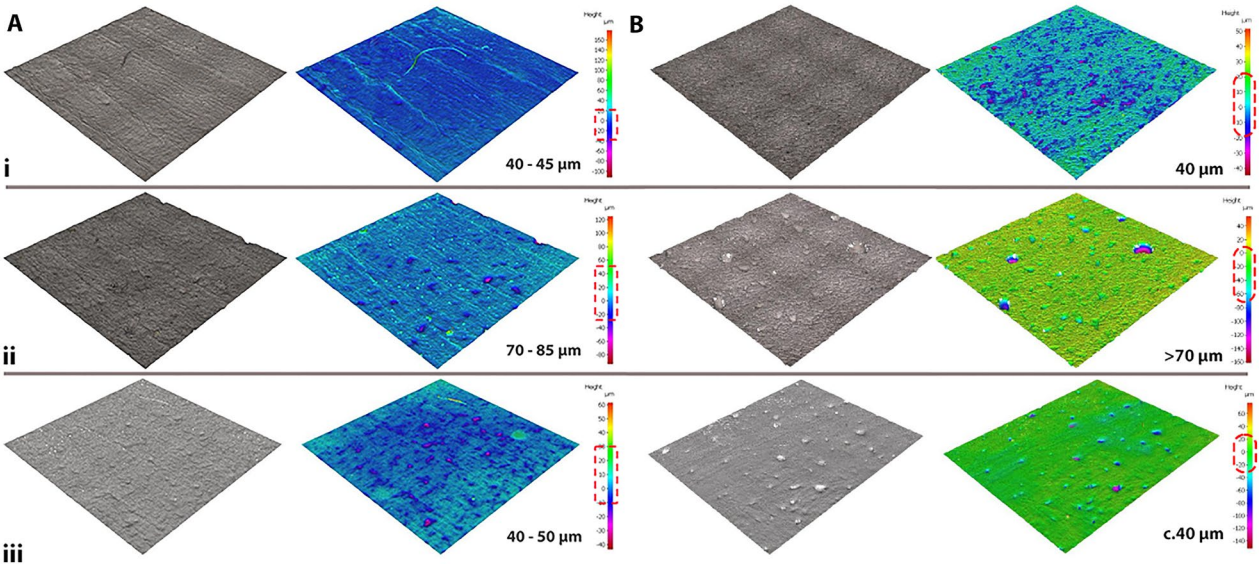

Fig. 6 HR 3D scans of 5.3 × 5.3 mm of an (**A**) aged beeswax coated (WX) and (**B**) uncoated plaster (uc) plate: (i) without soils, (ii) with soils and (iii) after the cleaning trial of 1 min contact with the PE-PAM_{15} loaded with 70% v/v IMS in DI water. The maps at the right demonstrate that the SAG system tend to restore the surface roughness of the plates that had been increased due to the soiling deposits

cleaning, but appeared higher than the roughness of the unsoiled surface.

The reduction of soil particles from all plate types was indicated by all data from BSE-SEM, digital optical, and HR 3D microscopy, corroborating the efficacy of the SAG cleaning procedure. Yet, the degree of removal is dependent on the nature of the coating, as the cleaning proved to be more effective on the beeswax coating that formed a film on top of the plaster surface compared to all other coatings that had infiltrated the substrate.

UV/Vis spectrophotometry of aged, soiled and cleaned plates

To assess changes in reflectance and scatter of the surfaces at the different stages of the experiments, UV/Vis spectrophotometry was employed. The spectrophotometric study along the 360–740 nm wavelength range revealed that the PE-PAM_{15} hydrogels reduced the overall reflectance of the soiled plates significantly compared to the reflectance prior to cleaning which was increased due to intense scattering [34] (Fig. 8).

The spectra indicate the chalky colour of all plates, while the reduced spectral line in the violet and blue part of the spectrum (360–495 nm) that slightly extents to the green (495–570 nm) indicates the yellowish hue of the plates. The cleaned plates approached the reflectance of the unsoiled plates because of reduced scattering compared to the soiled plates, which proves that the roughness of the uncoated and most of the coated plates was restored to a satisfactory degree after the cleaning tests, in line with the HR 3D microscopy study (Fig. 7). More specifically, the post cleaning spectra of plates with the boiled linseed oil, BL, and barite—$Ca(OH)_2$, BC, coatings are almost identical with their corresponding unsoiled plates. The same is observed for the plates coated with 18 wt% shellac in IMS, SR18, and neat barite, BA, although the spectral line is below that of the unsoiled plates by a small percentage, indicating minor smoothing in a good agreement with the roughness information discussed above. The rest of the plates including, cold pressed linseed oil (CL), 6 wt% shellac (SR6), beeswax (WX) and the uncoated (uc) plaster plate also exhibit reduced reflectance after cleaning that lies between the spectra of the soiled and unsoiled plates. The reflectance and scatter assessment are in line with the aforementioned analytical techniques, all confirming the effectiveness of the cleaning method.

Colourimetry, yellowness and gloss

As the overall appearance of heritage objects critically depend on visual perception of gloss and colour including yellowness as a subjective quality of ageing, colorimetric and gloss studies were performed on the plaster models to evaluate the impact of the SAG cleaning process on these visual qualities. The reflectance characteristics of the samples from the colourimetry study are summarized in Additional file 1: Table S2. The plots of colour difference ΔE_{00} [28] between soiled and cleaned plates and the yellowness index YI_{313} [29] are shown (Fig. 9). A detailed database is available [23]. The colour differences after

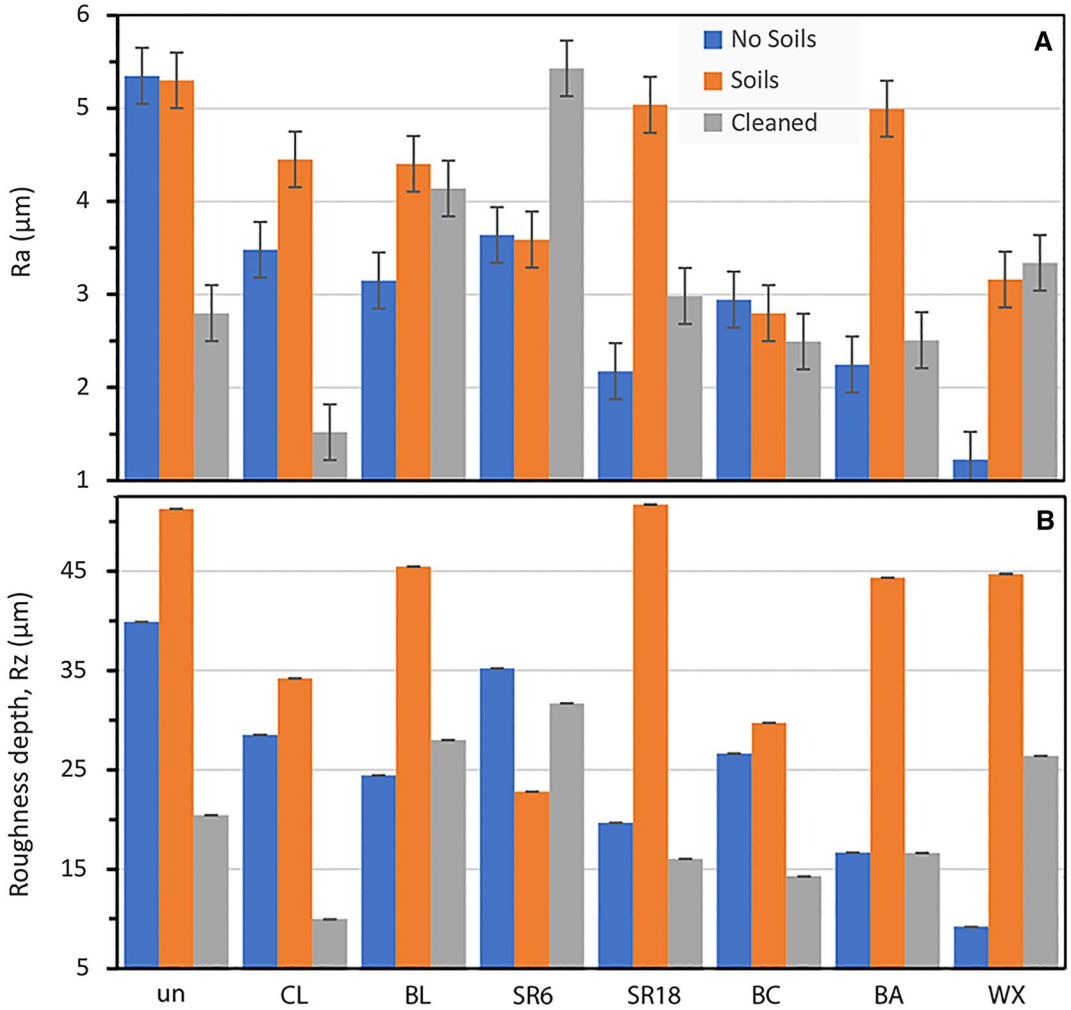

Fig. 7 Roughness, Ra (**A**) and roughness depth, Rz (**B**) of all coated, uncoated and cleaned samples

cleaning with the PE-PAM_{15} SAGs were not significant, with the maximum difference being that of cold pressed linseed oil (CL). Plates coated with both 6 wt% and 18 wt% shellac coatings (SR6, SR18) and beeswax (WX) had minor colour differences after cleaning, since the ΔE_{00} values were about or slightly above 1, which is the smallest noticeable colour difference [28]. The yellowness index YI_{313} [29] indicated that soiling followed by light exposure enhanced yellowing of all coated and uncoated (uc) plates. The removal of soils with the PE-PAM_{15} systems slightly reduced yellowing in all plates, but because of the light-induced discolouration of the organic phase of the soiling mixture, which includes inorganic particles, starch and gelatine in mineral oil [26], the cleaned areas were more yellow than the unsoiled plates (Fig. 9). On the other hand, the 1-min PE-PAM_{15} contact slightly increased the gloss of all surfaces within the matt range with the beeswax coated (WX) plate being affected the most (Additional file 1: Table S2, Fig. 9). However, all plates retained their matt appearance since all readings were less than 10 GU. The colour and gloss readings showed that the appearance of the SAG-cleaned surfaces was significantly improved.

ATR/FTIR and FTIR imaging of the aged and soiled plates

Changes in the chemical compositions of the coated and uncoated plaster surfaces due to SAG cleaning can be monitored by variation of characteristic bands in IR spectroscopy. Therefore, ATR/FTIR and FTIR Imaging were employed. IR reflectance measurements of the plaster plates acquired with the FTIR microscope previously, and provided in the database in reference [23], did not generate conclusive data for the impact of the soiling or the efficacy of the cleaning trials with PE-PAM_{15}. Therefore ATR/FTIR was directly acquired on the surface of

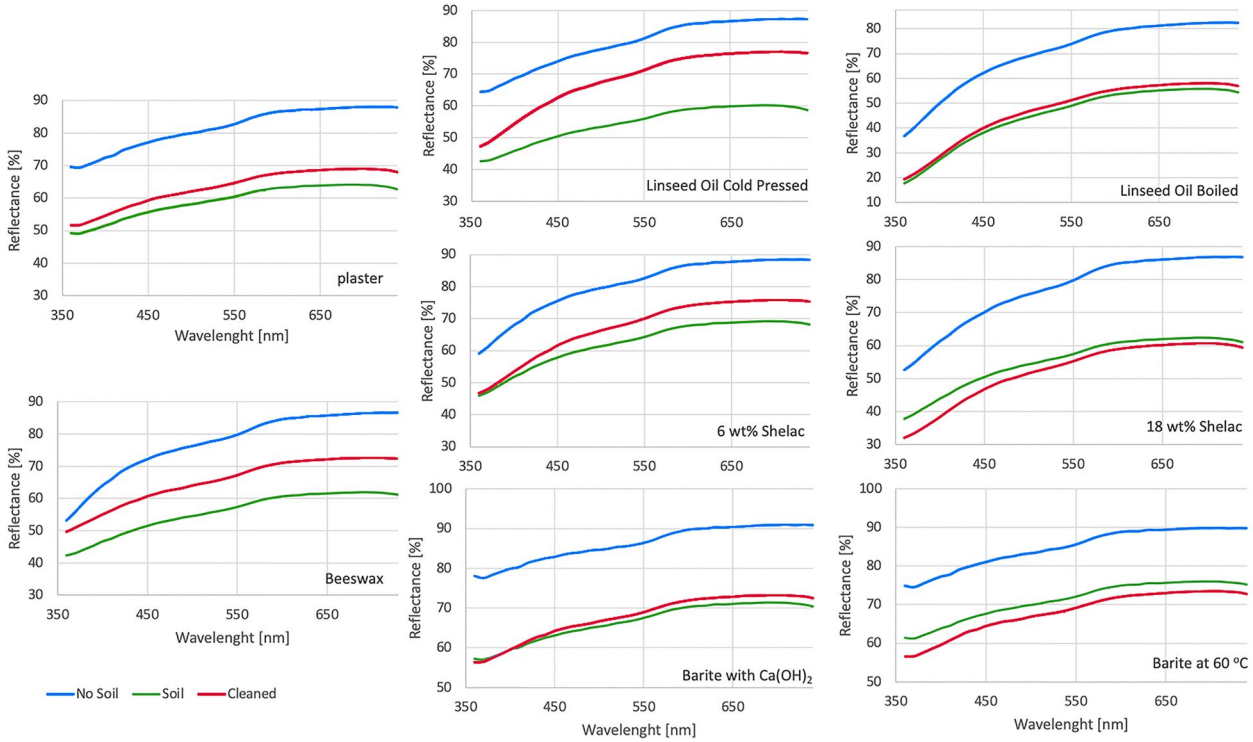

Fig. 8 The UV/VIS spectra of the aged plaster plates prior to soiling, after the deposition of soils and after 1 min contact with the PE-PAM$_{15}$ SAGs demonstrate a significant reduction of scattering post-cleaning

the uncoated (uc) and the coated plates before and after the cleaning tests.

ATR/FTIR demonstrated that all coatings except for the beeswax (WX) were absorbed by the substrate and therefore all plates had the characteristic bands of gypsum, $CaSO_4{\cdot}2H_2O$ (Additional file 1: Table S3, Fig. 10), including peaks at 3520, 3400 and 3233 cm^{-1} due to stretching vibration of hydroxyl groups in water, which were also detected at 1680, 1620 cm^{-1} due to bending vibrations [35, 36], a weak broad band at 2118–2248 cm^{-1} due to O-S-O stretching vibrations in sulphates, which were also monitored at the strong and broad peak at 1105 cm^{-1} due to O-S-O asymmetric stretching, a sharp spike at 1005 cm^{-1} due to O-S-O symmetric stretching, the sharp peaks at 667 and 597 cm^{-1} due to O-S-O bending and the frequencies 420–450 cm^{-1} due to O-S-O stretching vibrations [35, 37, 38]. The ATR/FTIR spectra of the linseed oil (CL, BL) and shellac (SR6, SR18) coated plates showed some bands of the corresponding coatings, which appeared weak due to the dominance of gypsum on the coated substrate. These were weak peaks at 2930 cm^{-1} (both linseed oil and shellac coatings), 2857 cm^{-1} (shellac) due to symmetric stretching of methyl and methylene groups respectively, at 1740 cm^{-1} (linseed oil) and 1722 cm^{-1} (shellac) both due to carbonyl stretching [35, 39]. Shellac (SR6, SR18) also presented peaks at 1458–1463 cm^{-1} due to methyl and methylene bending, 1399 cm^{-1} due to methyl bending and 1297 cm^{-1} due to ester bond stretching [35]. These observations were made in both the cold pressed (CL) and boiled linseed oil (BL) coatings, but the bands were better developed in the cold pressed linseed oil. Similarly, both concentrations of shellac resin coatings, namely 6 wt% and 18 wt% in IMS (SR6, SR18) generated the same peaks of the resin. The barite coating with the $Ca(OH)_2$ admixture (BC) generated strong calcite and aragonite signals with the most characteristic being the broad and strong peak at 1410 cm^{-1} due to C-O stretching of carbonate of calcite indicating the contamination of the coating with atmospheric CO_2 [40]. Calcite C-O vibrations of carbonate groups were also detected at 1066 cm^{-1} (stretching), 875 cm^{-1} (bending) and 713 cm^{-1} (bending) [35]. The peak at 713 cm^{-1} also includes C-O bending vibrations of carbonate from aragonite that also detected at 856 cm^{-1} due to out-of-plane bending vibrations [41]. The contribution of barites in the coating over the gypsum substrate was not detectable by FTIR, since the main sulphate bands are the same [42], but the hydroxide bands were weaker, as the bound water content of gypsum (calcium sulphate hydrates) were covered by the barite coating. Beeswax (WX) generated a thick coating over the plaster surface and therefore the ATR/FTIR spectra were characteristic of beeswax [35].

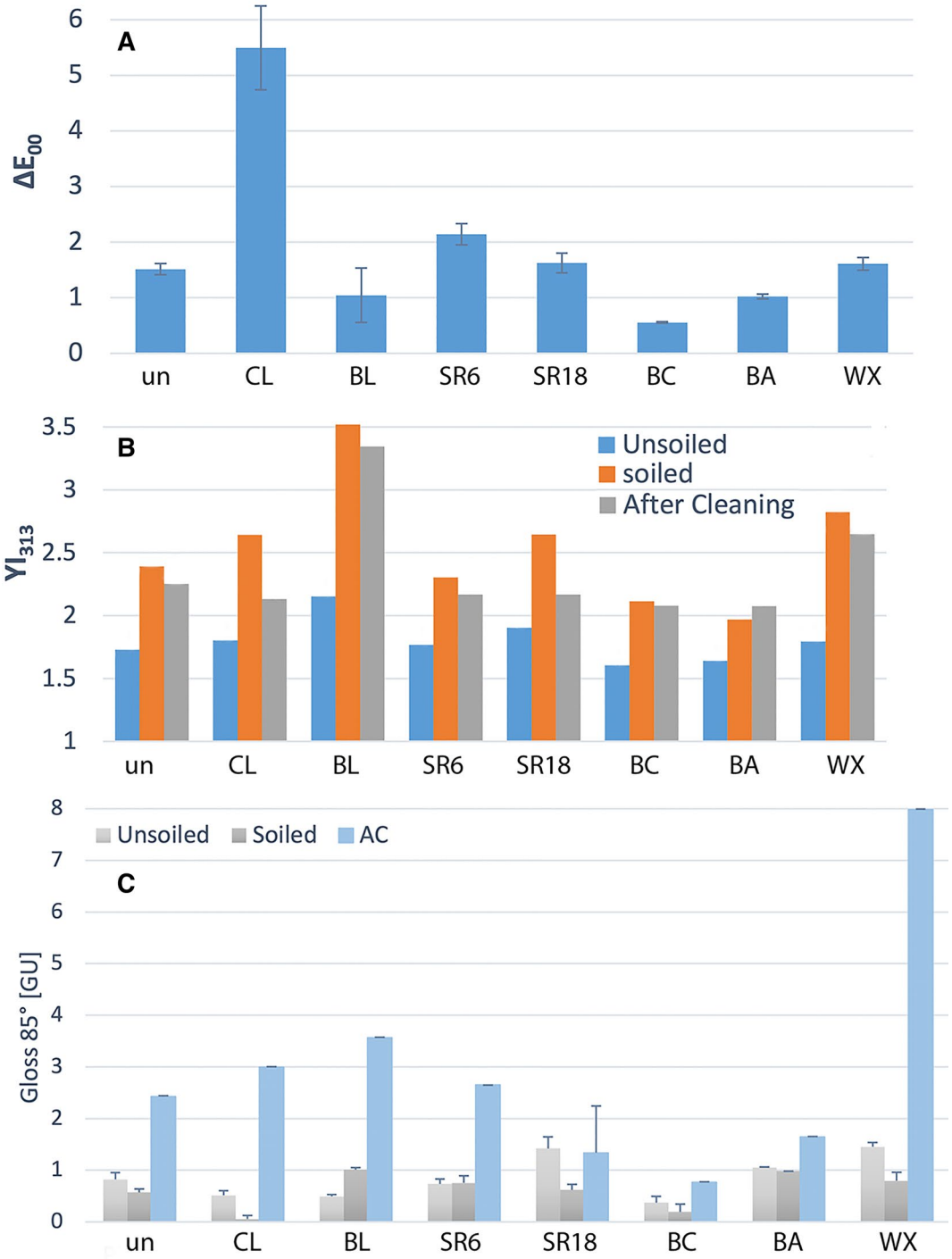

Fig. 9 Colour (**A**), yellowing (**B**) and gloss (**C**) of the aged plaster plate surfaces before and after the PE-PAM_{15} SAGs cleaning trials. **A** no significant colour change observed above the minimum noticeable difference ($\Delta E_{00} \approx 1$) with the exception of the cold pressed linseed oil coating. **B** Soiling increased the yellowness of all plates, while the PE-PAM_{15} cleaning tests slightly reduced it, and (**C**) Contact with the PE-PAM_{15} gels slightly increased gloss of all surfaces, although all samples remained matt (< 10 GU)

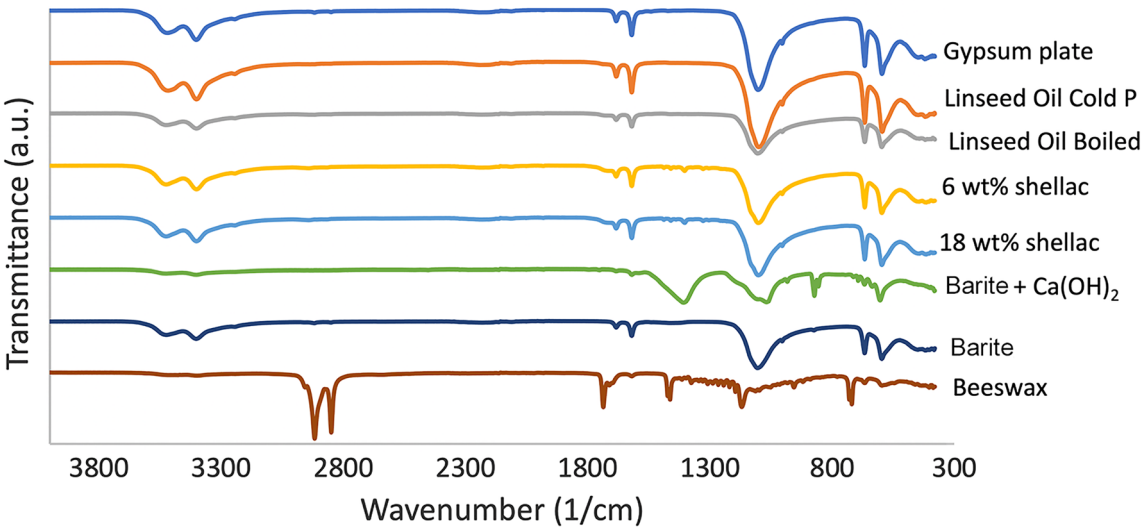

Fig. 10 ATR/FTIR of the plates prior to soiling. Except for the beeswax coated plates all other plates show the characteristic gypsum bands (Additional file 1: Table S3) indicating the absorption of the coatings into the gypsum substrate. Linseed oil (CL and BL) and shellac resin coated plates (SR6 and SR18) have a carbonyl signal at 1740 and 1722 cm^{-1} that appears as a shoulder of the weak band at 1680 cm^{-1} due to O-H bending of gypsum, and the barite-$Ca(OH)_2$ (BC) has characteristic peals of calcite at 1410 cm^{-1}, 1066 cm^{-1}, 875 cm^{-1} and aragonite at 856 cm^{-1} and 713 cm^{-1}. Beeswax (WX) generated a film over the plaster substrate

These included strong signals of C-H stretching (2954, 2917 and 2849 cm^{-1}) and C-H bending (1460, 1168 and 720 cm^{-1}) vibrations and a sharp C-O stretching band at 1168 cm^{-1} [43], with a minor interference of the underlying gypsum spectra, which are limited at a very weak spectral signal at 3520 and 3400 cm^{-1} (O-H stretch), a spike at 1620 cm^{-1} (O-H bending), a weak and broad peak at 1100 cm^{-1} (O-S-O stretch) and two low peaks at 667 and 597 cm^{-1} (O-S-O bending) which were much stronger in the rest of the plates.

The dispersed soils on the samples had no effect on the predominant bands of the gypsum substrate with the ATR/FTIR, but weakened the characteristic peaks of the coatings, some of which were not detectable after soiling (Fig. 11). In particular, the carbonyl stretching vibration bands at 1740 cm^{-1} of the CL and BL linseed oil coatings [35] or at 1722 cm^{-1} of the SR6 and SR18 shellac [39] coatings were significantly weaker, and the hydrocarbon bands (1458–1463, 1399 cm^{-1}) and ester bond peaks (1297 cm^{-1}) of shellac were not detected after soiling (Fig. 11). The barite and $Ca(OH)_2$ coating (BC) presented subtle differences with the most apparent one being the peak at 875 cm^{-1} that was less intense than the peak at 856 cm^{-1}, both being bending of carbonate of calcite [40] and aragonite [41] respectively, compared to the respective unsoiled plate. The other plates did not present detectable changes after soiling by ATR/FTIR.

The efficacy of the PE-PAM_{15} systems to remove soils from the uncoated plaster (uc) and the coated plaster surfaces was demonstrated in the ATR/FTIR spectra of the linseed oil (CL, BL), shellac (SR6, SR18) and barite-$Ca(OH)_2$ (BC) coated plates which showed that the respective hydrocarbon, carbonyl and carbonate bands were restored after cleaning (Fig. 11). FTIR imaging maps of the soiled samples with these particular coatings produced a wider range of absorbance intensities than the maps of the same samples before soiling and after the cleaning trials with the PE-PAM_{15} SAGs. All data are available in a comprehensive database [23]. The ATR/FTIR measurements showed that the dispersed soils on the surface of plates weakened or obscured the characteristic peaks of the coatings, so some of which were not detectable after soiling. Since the spectra of the plates after cleaning were similar to the spectra of the plates before soiling, effective SAG cleaning is clearly proven by these experiments.

Furthermore, FTIR imaging confirmed the ATR/FTIR observation, as shown in Fig. 11, illustrating an example of how soiling obscures the average reflectance maps, in particular for linseed oil, shellac and the barite-$Ca(OH)_2$ coatings. In agreement with ATR/FTIR measurement, the FTIR maps of the plates after SAG cleaning were very similar to the ones before soiling. Again, this observation provides a good argument for the efficacy of the SAG-induced soil removal.

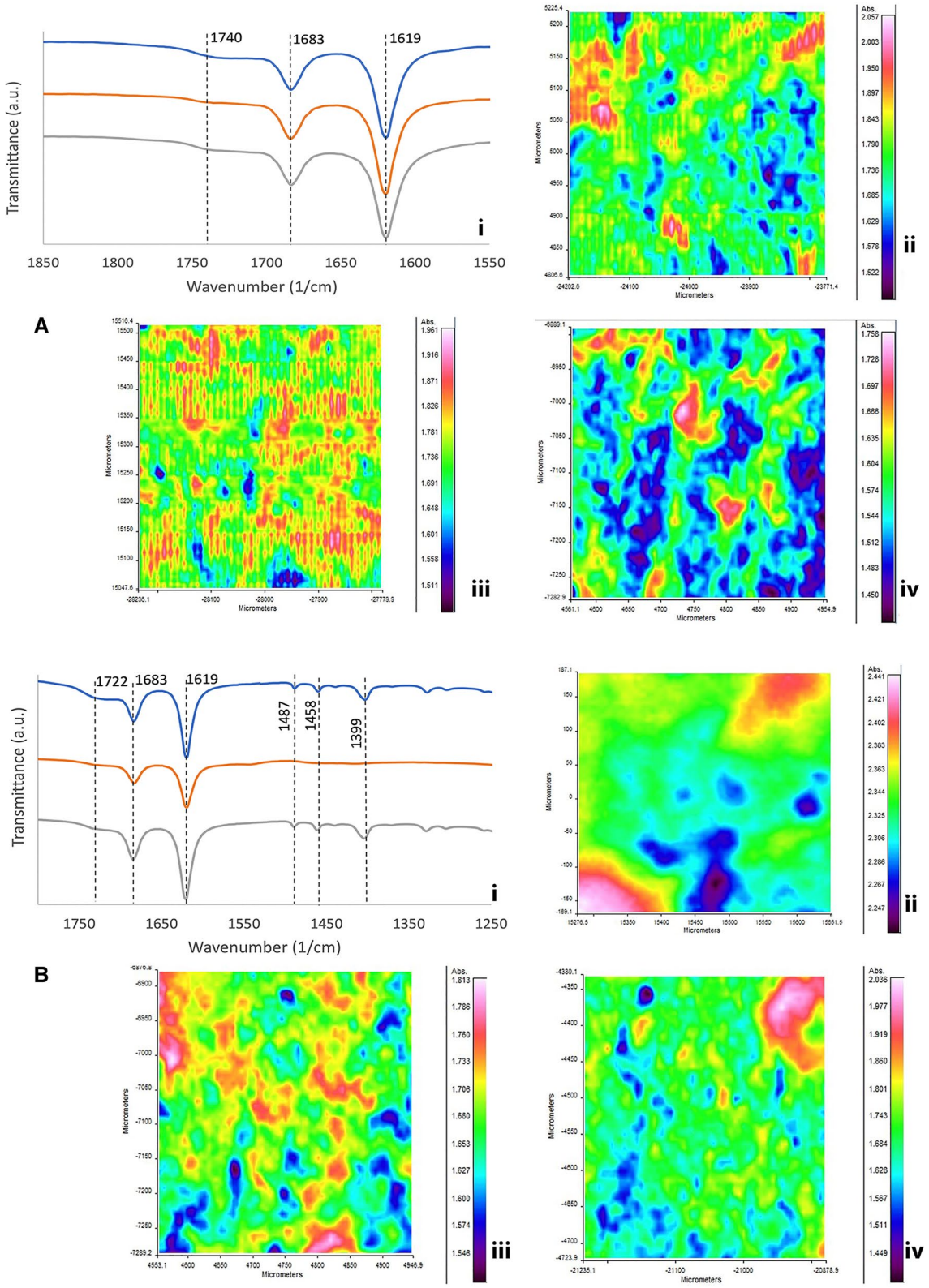

Fig. 11 ATR/FTIR (4000–350 cm^{-1}) (i) and 2D microFTIR Imaging (4000–650 cm^{-1}) (ii-iv) of coated plaster plates with: **A** cold pressed linseed oil (CL), **B** 6 wt% shellac in IMS (SR6) and **C** Barite-$Ca(OH)_2$ admixture (BC), before soiling (blue line in (i), image (ii), after soiling (orange line in (i), image (iii) and after cleaning (grey line in (i), image (iv). Refer to Additional file 1: Table S3 for the band assignments

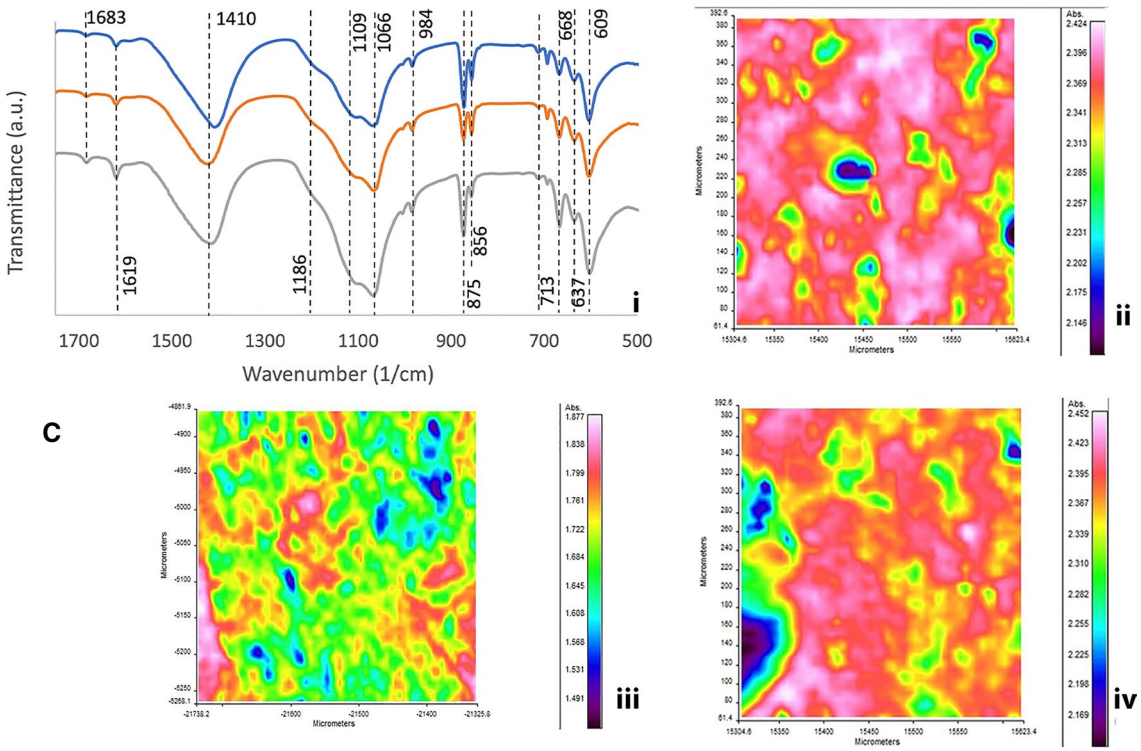

Fig. 11 continued

Conclusions

The experimental results in this paper clearly demonstrate that the application of SAGs consistently facilitated remarkable removal of soils from the plaster surfaces. The SAGs worked very efficiently, despite the variability of the sample types comprising uncoated and the coated gypsum plaster plates with substantial differences in chemical surface composition. The cleaning trials were performed on gypsum plaster surfaces with or without organic and inorganic coatings with thin 15-min photocrosslinked poly(acrylamide-co-benzophenyl acrylamide) films that were covalently attached on flexible polyethylene foils (PE-PAM_{15}) and swollen in effective solvents customized for each specific substrate. One-minute contact of the solvent-swollen SAG hydrogels followed by dry cotton swab roll was sufficient to remove soils from the uncoated gypsum plaster and plaster plates with coatings such as aged linseed oil, shellac resin, barites and beeswax. SAGs exhibited fast and minimal wetting of all surfaces tested, eventually preventing excessive spreading and slow liquid diffusion into water-sensitive gypsum substrates. The post-cleaning visual, morphological, and spectral evaluation did not detect damage to the water-sensitive gypsum substrates. As expected, the less porous coating of beeswax, which was the only coating that formed a complete film over the gypsum substrate, responded best to the SAG cleaning trials. Due to capillarity, the uncoated and the barite-coated substrates absorbed the solutions form the SAG faster than the other substrate types, potentially inducing minor dissolution and recrystallization. Yet, the cleaning results for these substrates were remarkable. As the linseed oil and shellac resin did not form a continuous film on top of the plaster, a relatively high surface roughness was retained, which reduced the conformal contact of the SAG hydrogel layer during SAG application. Nevertheless, impressive cleaning efficacy was also observed in these cases.

With these excellent cleaning results utilizing SAG hydrogel systems, this method could unfold novel approaches for the cleaning of historical plaster objects.

Supplementary Information

The online version contains supplementary material available at https://doi.org/10.1186/s40494-023-00924-5.

Additional file 1: Figure S1. Visible light and UV fluorescence of plaster plates that shows the coated plaster layout. In this example, the coatings are made of shellac 6wt% and 18wt% in IMS. Plate **C** is coated with beeswax on top of the shellac coatings, whereas plate **A** does not have the beeswax coating. The upper half of the plates is soiled. A detailed database of the VR and UVf images is available [21]. **Figure S2**. Agarose plugon plaster substrate used to measure pH and conductivity. Note that the camera lens focused on the reflection of the agarose plug on the gypsum surface. **Figure S3**. Preliminary tests on a soiled plaster plated

coated with boiled linseed oil. The marked areas show the tests with: PE-PAM_{15}, PE-PAME3-15 loaded with a pH 8.5 aqueous solution after 1 minute contact, showing the same cleaning capacity, swab rolling that used to indicate the suitability of the solution. The area shows the spot where pH and conductivity of the plate was measured. The central area shows a 2x2 cm PE-PAM15 SAG foil on the plate. **Figure S4**. ATR-FTIR spectra of the neat barite coatingand the Barite-Ca2 coatingon the gypsum surfaces. Both spectra have strong contributions from sulfates as shown at peaks 1105, 1005, 667 and 597 cm-1. The Barite-Ca2 coated surface shows strong peaks that are characteristic to carbonates at 1410, 1066, 875 and 856 cm-1, as shown in Table 3s. **Figure S5**. ATR-FTIR spectrum of the neat barite coating on gypsumand single wavenumber FTIR spectral maps. FTIR Imaging determined the presence of sulfates at 2240, 1105 and 1005 cm-1 and the absence of carbonates. **Figure S6**. ATR-FTIR spectrum of the barite-Ca2 coating on gypsum and single wavenumber FTIR spectral maps. FTIR Imaging determined the presence of sulfates at 2240, 1105 and 1005 cm-1 and carbonates at 1410, 1065, 875 and 856 cm-1. **Table S1**. Roughness, Ra, and roughness depth, Rz. **Table S2**. Colourimetry and gloss data. **Table S3**. FTIR bands and relevant assignments of the spectra acquired from unsoiled, soiled and cleaned uncoated and coated plaster plates.

Acknowledgements
Special thanks to the V&A Sculpture Conservation team and the V&A Science team.

Author contributions
CT and UJ conceived and designed SAGs. UJ, SF, and SD designed synthesis experiments, polymer synthesis, polymer characterization, fabrication of SAGs. CT and VR conceived, designed and performed the cleaning experiments; CT and VR designed analysis and analyzed the data; CT wrote the manuscript. CT, VR, SF and UJ reviewed the manuscript and agreed on revisions. All authors have read and agreed to the published version of the manuscript. All authors read and approved the final manuscript.

Funding
This research was funded by the Art and Humanities Research Council (2017-21 AHRC/CDP Northumbria University and Victoria and Albert Museum-AH/R00322X/1) and supported by the Henry Moore Foundation (HMF Research and Travel Grant-2018).

Availability of data and materials
Data are available in the supporting information and in the database cited in this paper [23].

Declarations

Ethics approval and consent to participate
Not applicable.

Consent for publication
All co-authors consent.

Competing interests
Not applicable.

Received: 13 November 2022 Accepted: 4 April 2023
Published online: 15 May 2023

References

1. Ormsby B, Townsend J, Angelova LV, Wolbers R. Gels in the Conservation of Art. London: Archetype Publications; 2017.
2. Bonelli N, Poggi G, Chelazzi D, Giorgi R, Baglioni P. Poly(vinyl alcohol)/poly(vinyl pyrrolidone) hydrogels for the cleaning of art. J Colloid Interface Sci. 2019;536:339–48. https://doi.org/10.1016/j.jcis.2018.10.025.
3. Ormsby B, Kampasakali E, Miliani C, Learner T. An FTIR-based exploration of the effects of wet cleaning treatments on artists' acrylic emulsion paint films. Preserv Sci. 2009;6:186–95.
4. Berg KJ, Burnstock A, de Keijzer M, Krueger J, Learner T, de Tagle A, Heydenreich G. Issues in Contemporary Oil Paint. Amsterdam: Springer; 2015.
5. Burnstock A, White R. The effects of selected solvents and soaps on a simulated canvas painting. In: Mills JS, Smith P (eds). Cleaning, Retouching and Coatings. London: https://doi.org/10.1179/sic.1990.35.s1.024
6. Cremonesi P, Casoli A. Thermo-reversible rigid agar hydrogels: their properties and action in cleaning. In: Ormsby B, Townsend JH, Wolbers R, editors. Gels in the conservation of art. London: Archetype Publications; 2017.
7. Angelova LV, Leskes M, Berrie BH, Weiss RG. Selective formation of organo, organo-aqueous, and hydro gel-like materials from partially hydrolysed poly(vinyl acetate)s based on different boron-containing crosslinkers. Soft Matter. 2015;11(25):5060–6. https://doi.org/10.1039/C5SM00465A.
8. Domingues JAL, Bonelli N, Giorgi R, Fratini E, Gorel F, Baglioni P. Innovative hydrogels based on semi-interpenetrating p(HEMA)/PVP networks for the cleaning of water-sensitive cultural heritage artifacts. Langmuir. 2013;29(8):2746–55.
9. Wolbers R. Cleaning painted surfaces: aqueous methods. London: Archetype Publications; 2000.
10. Pizzorusso G, Fratini E, Eiblmeier J, Giorgi R, Chelazzi D, Chevalier A, Baglioni P. Physicochemical characterization of acrylamide/bisacrylamide hydrogels and their application for the conservation of easel paintings. Langmuir. 2012;28:3952–61.
11. Jonas U, Brom CR, Brunsen A, Roskamp RF. Surface attached polymeric hydrogel films. In: Knoll W, editor. Handbook of Biofunctional Surfaces. Singapore: Pan Stanford Publishing; 2012.
12. Kuenzler JF. Hydrogels. In: Mark HF, editor. Encyclopedia of Polymer Science and Technology. New York: Wiley-Interscience; 2004.
13. Caminati G. Cultural Heritage Artefacts and Conservation: Surfaces and Interfaces. In: Baglioni P, Chelazzi D, editors. Nanoscience for the conservation of works of art. Cambridge: RSC; 2013. p. 1–48.
14. Angelova LV, Ormsby B, Richardson E. Diffusion of water from a range of conservation treatment gels into paint films studied by unilateral NMR Part I: Acrylic emulsion paint. Microchem J. 2016. https://doi.org/10.1016/j.microc.2015.09.012.
15. Mateescu A, Freese S, Frank P, Jonas U, Theodorakopoulos C. Novel surface-attached gels from photo-crosslinkable polyacrylamides for the cleaning of works of art. In: Ormsby B, Townsend JH, Wolbers R, editors. Gels in the conservation of art. London: Archetype Publications; 2017.
16. Freese S, Diraoui S, Mateescu A, Frank P, Theodorakopoulos C, Jonas U. Polyolefin-supported hydrogels for selective cleaning treatments of paintings. Gels. 2020;6(1):1. https://doi.org/10.3390/gels6010001.
17. Voorhaar L, Hoogenboom R. Supramolecular polymer networks: Hydrogels and bulk materials. Chem Soc Rev. 2016;45:4013–31. https://doi.org/10.1039/C6CS00130K.
18. Risdonne V, Hubbard C, Borges VHL, Theodorakopoulos C. Materials and techniques for the coating of nineteenth century plaster casts: a review of historical sources. Stud Conserv. 2022. https://doi.org/10.1080/00393630.2020.1864896.
19. Graepler D, Ruppel J. Weiß wie Gips?: Die Behandlung der Oberflächen von Gipsabgüssen. In: 2016 Wissenschaftliche Fachtagung Archäologisches Institut Und Sammlung Der Gipsabgüsse. Göttingen, 13–15 Oktober 2016: VML Verlag Marie Leidorf; 2019
20. Bochen C, Slomka-Slupik B, Slusarek J. Experimental study on salt crystallization in plasters subjected to simulate groundwater capillary rise. Construct Building Mater. 2021. https://doi.org/10.1016/j.conbuildmat.2021.125039.
21. Hubbard C, Pretzel, B. A study of the use of latex cleaning product on historic plaster casts. Unpublished V&A internal report. Retrieved from Collection Management System. 2016.
22. Risdonne V. Materials and techniques for the coating of the nineteenth-century plaster casts a scientific and archival investigation of the Victoria Albert Museum cast collection. PhD thesis, Northumbria University. Newcastle, 2022.
23. Risdonne V, Theodorakopoulos C. Database: Materials and techniques for coating of the nineteenth-century plaster casts A scientific and archival investigation of the Victoria & Albert Museum cast collection. Newcastle: Northumbria University; 2021.

24. Risdonne V, Hubbard C, Puisto J, Theodorakopoulos C. A multi-analytical study of historical coated plaster surfaces: the examination of a nineteenth-century V&A cast of a tombstone. Herit Sci. 2021;9:70. https://doi.org/10.1186/s40494-021-00533-0.
25. Risdonne V, Miró AF, Morio S, Theodorakopoulos C. The victoria and albert museum plaster casts by the nineteenth-century workshops of the notre-dame cathedral: scientific analysis and conservation. Herit. 2022;5:3427–45. https://doi.org/10.3390/heritage5040176.
26. Galatis P, Boyatzis S, Theodorakopoulos C. Removal of a synthetic soiling mixture on mastic, shellac & Laropal® K80 coatings using two hydrogels. E-Preserv Sci. 2012;9:72–83.
27. BS EN ISO 16474-1:2013 Paints and varnishes—methods of exposure to laboratory light sources—Part 1: General guidance. 2013 https://www.iso.org/standard/56803.html
28. Hunt RWG, Pointer MR. Measuring Colour. United Kingdom: Wiley; 2011.
29. Henderson S. White gold alloys: colour measurement and grading. Gold Bulletin. 2005;38(2):55–67.
30. Kotwaliwale N, Bakane P, Verma A. Changes in textural and optical properties of oyster mushroom during hot air drying. J Food Eng. 2007;78(4):1207–11. https://doi.org/10.1016/j.jfoodeng.2005.12.033.
31. Aquilano D, Otálora F, Pastero L, García-Ruiz JM. Three study cases of growth morphology in minerals: Halite, calcite and gypsum. Prog Cryst Growth Charact Mater. 2016;62(2):227–51. https://doi.org/10.1016/j.pcrysgrow.2016.04.012.
32. Cox KG, Price NB, Harte B. An introduction to the practical study of crystals, minerals, and rocks. New Jersey: John Wiley & Sons; 1974.
33. Turco A. Il Gesso. Lavorazione, trasformazione, impieghi. Milano: Hoepli. 1990 ISBN: 9788820317065
34. Theodorakopoulos C, Zafiropulos V, Boon JJ, Boyatzis SC. Spectroscopic investigations on the depth-dependent degradation gradients of aged triterpenoid varnishes. Appl Spectrosc. 2007;61(10):1045–51. https://doi.org/10.1366/000370207782217833.
35. Derrick MR, Stulik D, Landry JM. Infrared spectroscopy in conservation science. Los Angeles: Getty Publications, 1999. ISBN 0-89236-469-6 http://hdl.handle.net/10020/gci_pubs/infrared_spectroscopy
36. Serafima S, Duliu OG, Manea MM, Niculescu G. FTIR, XRF and optical microscopy analysis of the painting layer of an early 19th-century icon. Rom Rep Phys. 2016;68(1):191–202.
37. Anastasiou M, Hasapis T, Zorba T, Pavlidou E, Chrissafis K, Paraskevopoulos KM. TG-DTA and FTIR analyses of plasters from byzantine monuments in Balkan region. J Therm Anal Calorim. 2006;84(1):27–32. https://doi.org/10.1007/s10973-005-7211-9.
38. Price BA, Pretzel B, Lomax SQ. Infrared and raman users group spectral database. Philadelphia: IRUG; 2007 http://www.irug.org/
39. de Viguerie L, Payard PA, Portero E, Walter P, Cotte M. The drying of linseed oil investigated by fourier transform infrared spectroscopy: Historical recipes and influence of lead compounds. Prog Org Coat. 2016;93:46–60. https://doi.org/10.1016/j.porgcoat.2015.12.010.
40. Blesa MJ, Miranda JL, Moliner R. Micro-FTIR study of the blend of humates with calcium hydroxide used to prepare smokeless fuel briquettes. Vib Spectrosc. 2003;33(1–2):31–5. https://doi.org/10.1016/S0924-2031(03)00089-4.
41. Michael BT, Regev L, Dubernet S, Lefrais Y, Boaretto E. FTIR-based crystallinity assessment of aragonite-calcite mixtures in archaeological lime binders altered by diagenesis. Minerals. 2019;9(2):121. https://doi.org/10.3390/min9020121.
42. Prameena B, Anbalagan G, Sangeetha V, Gunasekaran S, Ramkumaar GR. Behaviour of Indian natural Baryte mineral. Int J Chemtech Res. 2013;5(1):220–31.
43. Bucio A, Moreno-Tovar R, Bucio L, Espinosa-Dávila J, Anguebes-Franceschi F. Characterization of beeswax, candelilla wax and paraffin wax for coating cheeses. Coatings. 2021;11(3):261. https://doi.org/10.3390/coatings11030261.

Publisher's Note